MECHANIKA TEORETYCZNA
I STOSOWANA
Journal of Theoretical
and Applied Mechanics
1, 35, 1997

DYNAMIC MODEL OF BEAM-PIEZOCERAMIC ACTUATOR COUPLING FOR ACTIVE VIBRATION CONTROL

MAREK PIETRZAKOWSKI

Institute of Machine Design Fundamentals, Warsaw University of Technology
e-mail: mpi@simr.pw.edu.pl

In the paper the piezoelectric sensor/actuator pair capable of controlling structural vibrations of a simply supported beam has been analysed. The dynamic model of the beam-actuator coupling which includes the shear bonding layer is developed by taking into account the bending effect of the actuator. Solving the boundary value problem and assuming a harmonic excitation by the applied voltage, the transfer functions for the uncontrolled beam as well as for the system with velocity feedback are obtained. The numerical results prove the influence of bonding layer properties on frequency response functions. The results based on the proposed model of dynamic coupling are compared with those one obtained in the case the bending of the actuator is neglected.

Key words: active vibration control, piezoelectric element

1. Introduction

Piezoelectric distributed actuators and sensors have been applied succesfully to the vibration control of flexible structures. Dynamic analysis of beams and one-dimensional plates is commonly based on the Bernoulli-Euler theory and the assumption of static coupling with zero glue layer thickness between the piezoelectric element and the substructure (cf Bailey and Hubbard (1985); Clarc et al. (1991); Newman (1991); Lee et al. (1991); Pietrzakowski (1993)). A comprehensive static model of the beam-actuator coupling which includes an elastic bonding layer was analysed by Crawley and de Luis (1987). The relationship between the strain distributions, both on the surface of the beam and in the actuator caused by the applied voltage was demonstrated. The dynamic behaviour of the coupled system predicted using the static approach was compared with the results of dynamic modelling obtained by Jie Pan et

al. (1991). Assuming the perfect bonding the differences between the strain distributions were shown. A more advanced dynamic model including the bonding layer with the finite stiffness was presented and discussed by Tylikowski (1993).

In this paper the model of the beam-bonding layer-actuator system based on the approach proposed by Tylikowski is formulated. Dynamic longitudinal strain on the beam surface is calculated by considering the dynamic coupling between actuator and substructure, by imposing the free stress conditions on the actuator boundaries, and by including the adhesive material layer with a finite stiffness. The dynamic model is also developed by taking into account the bending effect of the piezoelectric actuator. The proposed model of dynamic coupling is applied to the vibration control system used to achieve active damping of the structure. The results obtained here are compared with those obtained by neglecting the deflection of the actuator.

2. Formulation of the problem

The system considered herein is a simply supported beam with piezoelectric patches symmetrically bonded to both opposite sides as shown in Fig.1. The upper piezoceramic element acts as an actator and is mounted by a finite-thickness bonding layer to the elastic substructure. The lower piezoelectric film is assumed to be perfectly bonded with zero glue layer thickness and is used for sensing.

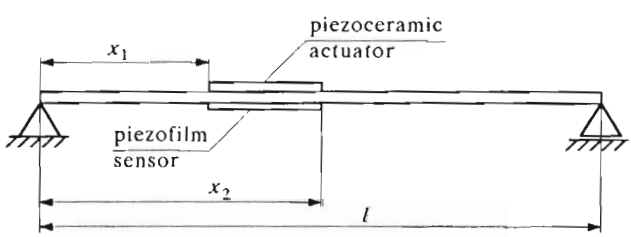

Fig. 1. Beam with a piezoelectric actuator/sensor pair

Dynamic analysis of the system is based on the Bernoulli-Euler beam theory. Due to the geometry, the beam, is divided into three sections, for which dynamic relation are formulated separately. To obtain the dynamic coupling between the actuator and the beam, according to the approach presented by Tylikowski, the pure 1D shear in the isotropic bonding layer is assumed.

An element of dx length in the second section of the beam $x_1 < x < x_2$ and acting forces and moments are presented in Fig.2. The thicknesses of beam, bounding layer, piezoelectric actuator and sensor are denoted by t_b, t_s, t_a, t_f, respectively. The sensor is analysed together with the substructure since the piezofilme thinness $t_f \ll t_b$.

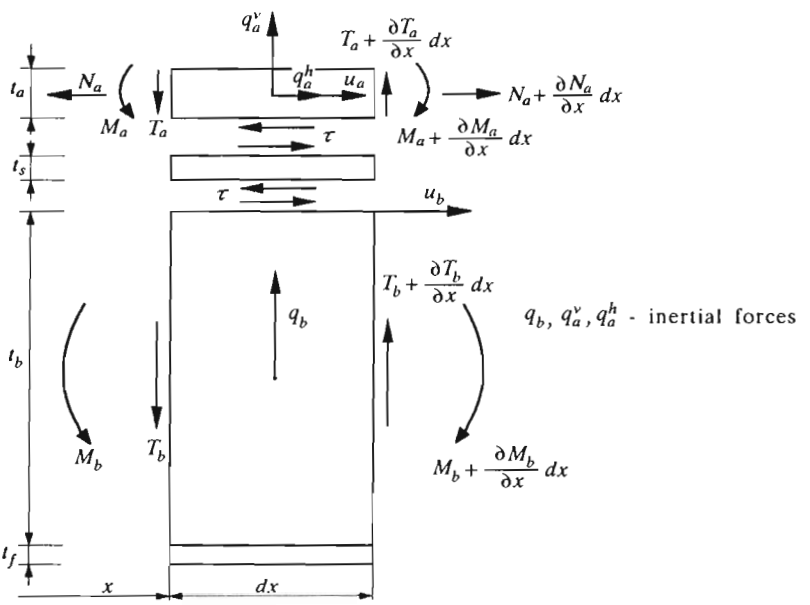

Fig. 2. Geometry of a beam element with piezoelectric and bonding layers, and acting forces and moments

When applying an electrical field to the actuator, displacements u_a, u_{ab}, u_b and shear stress τ are generated. The surface displacement u_{ab} is caused by the piezoceramic deflection which relates to the deflection of the beam.

The longitudinal motion of the actuator is given by the equation

$$\frac{\partial \sigma_a}{\partial x} t_a - \tau - \rho_a t_a \frac{\partial^2 u_a}{\partial t^2} = 0 \tag{2.1}$$

where

σ_a – uniform tensile stress

ρ_a – denotes the material density.

The stress-strain relation for the piezoelectric element has the form (cf Crawley and de Luis (1987))

$$\sigma_a = E_a(\varepsilon_a - \lambda) \tag{2.2}$$

where

E_a – Young modulus

ε_a – longitudinal strain, $\varepsilon_a = \partial u_a/\partial x$

λ – strain of the unconstrained element induced by the voltage V along its polarization direction

$$\lambda = \frac{d_{31}V}{t_a} \tag{2.3}$$

and d_{31} is the piezoelectric strain constant.

The shear stress τ on the interface causes the beam deflection. Denoting the transverse displacement by w the beam dynamic equations can be written as

$$\begin{aligned} &\frac{\partial T_b}{\partial x} - \rho_z t_z b \frac{\partial^2 w}{\partial t^2} = 0 \\ &\frac{\partial M_b}{\partial x} - T_b + \tau b \frac{t_b}{2} = 0 \end{aligned} \tag{2.4}$$

where

T_b – shear force

M_b – bending moment

b, t_z – dimensions of the coupled beam and piezofilm cross section, respectively, $t_z = t_b + t_f$

ρ_z – equivalent density, $\rho_z = (\rho_b t_b + \rho_f t_f)/t_z$.

The bending moment-beam surface strain relation can be specified as

$$M_b = \frac{E_b t_b^2 b}{6}\varepsilon_b \tag{2.5}$$

where ε_b is equal to $\varepsilon_b = \partial u_b/\partial x$.

Geometric relations of the deformed beam lead to the following formula

$$\frac{\partial^2 w}{\partial x^2} = -\frac{2\varepsilon_b}{t_b} \tag{2.6}$$

Assuming deflection of the actuator the same as that of the beam, the actuator surface strain $\varepsilon_{ab} = \partial u_{ab}/\partial x$ is related to the beam surface strain ε_b by

$$\varepsilon_{ab} = \frac{t_a}{t_b}\varepsilon_b \tag{2.7}$$

The actuator dynamic equations describing the bending effect are formulated as follows

$$\begin{aligned} &\frac{\partial T_a}{\partial x} - \rho_a t_a b \frac{\partial^2 w}{\partial t^2} = 0 \\ &\frac{\partial M_a}{\partial x} - T_a + \tau b \frac{t_a}{2} = 0 \end{aligned} \tag{2.8}$$

The bending moment M_a can be represented by a relation of the actuator surface strain ε_{ab} by

$$M_a = \frac{E_a t_a^2 b}{6} \varepsilon_{ab} \tag{2.9}$$

The shear stress on a massless bonding layer is determined by the equation

$$\tau = \frac{G}{t_s}(u_a - u_{ab} - u_b) \tag{2.10}$$

where G is the shear modulus.

By adding Eqs $(2.4)_1$ and $(2.8)_1$ and Eqs $(2.4)_2$ and $(2.8)_2$, respectively, after eliminating displacements w, u_b, u_a, u_{ab}, inner forces and moments and shear stress τ, the equations of motion of the second section of the beam and of the actuator can be expressed in beam surface strain ε_b and pure longitudinal strain ε_a as follows

$$\begin{aligned} &\frac{E_b t_b^2}{6}\gamma \frac{\partial^4 \varepsilon_b}{\partial x^4} + \rho_c \frac{t_c}{t_b}\frac{\partial^2 \varepsilon_b}{\partial t^2} + \frac{G t_b}{4 t_s}\beta\Big(\frac{\partial^2 \varepsilon_a}{\partial x^2} - \beta \frac{\partial^2 \varepsilon_b}{\partial x^2}\Big) = 0 \\ &E_a t_a \frac{\partial^2 \varepsilon_a}{\partial x^2} - \rho_a t_a \frac{\partial^2 \varepsilon_a}{\partial t^2} - \frac{G}{t_s}(\varepsilon_a - \beta \varepsilon_b) = 0 \qquad x \in (x_1, x_2) \end{aligned} \tag{2.11}$$

where

$$\gamma = 1 + \frac{E_a}{E_b}\Big(\frac{t_a}{t_b}\Big)^3 \qquad \beta = 1 + \frac{t_a}{t_b}$$

$$\rho_c = \frac{\rho_z t_z + \rho_a t_a}{t_c} \qquad t_c = t_z + t_a$$

The dynamic equations for the first and third sections of the beam are obtained using the clasical beam theory and become

$$\begin{aligned} &\frac{E_b t_b^2}{12}\frac{\partial^4 \varepsilon_{b1}}{\partial x^4} + \rho_b \frac{\partial^2 \varepsilon_{b1}}{\partial t^2} = 0 \qquad x \in (0, x_1) \\ &\frac{E_b t_b^2}{12}\frac{\partial^4 \varepsilon_{b3}}{\partial x^4} + \rho_b \frac{\partial^2 \varepsilon_{b3}}{\partial t^2} = 0 \qquad x \in (x_2, l) \end{aligned} \tag{2.12}$$

where unknown functions $\varepsilon_{b1}(x,t)$, $\varepsilon_{b3}(x,t)$ denote the surface strain for the beam sections 1 and 3, respectively.

In the solution of the system equations the geometrical, continuity and free stress conditions, respectively, are formulated in terms of strain. The boundary conditions corresponding to the simply supported edges are given by

$$\begin{aligned} &\iint \varepsilon_{b1}\, dxdx\Big|_{x=0} = \iint \varepsilon_{b3}\, dxdx\Big|_{x=l} = 0 \\ &\varepsilon_{b1}(0,t) = \varepsilon_{b3}(l,t) = 0 \end{aligned} \tag{2.13}$$

The continuity of beam deflection and slope at $x = x_1$ and $x = x_2$ leads to the equations

$$\begin{aligned} &\iint \varepsilon_{b1}\, dxdx\Big|_{x=x_1} = \iint \varepsilon_b\, dxdx\Big|_{x=x_1} \qquad \int \varepsilon_{b1}\, dx\Big|_{x=x_1} = \int \varepsilon_b\, dx\Big|_{x=x_1} \\ &\iint \varepsilon_b\, dxdx\Big|_{x=x_2} = \iint \varepsilon_{b3}\, dxdx\Big|_{x=x_2} \qquad \int \varepsilon_b\, dx\Big|_{x=x_2} = \int \varepsilon_{b3}\, dx\Big|_{x=x_2} \end{aligned} \tag{2.14}$$

The continuity condition for curvature or bending moment has the form

$$\varepsilon_{b1}(x_1,t) = \varepsilon_b(x_1,t) \qquad \varepsilon_b(x_2,t) = \varepsilon_{b3}(x_2,t) \tag{2.15}$$

The continuity condition for transverse force at the borders of the sections can be expressed by the following relations

$$\begin{aligned} &\frac{E_b t_b^2}{6}\frac{\partial \varepsilon_{b1}}{\partial x}\Big|_{x=x_1} = \frac{E_b t_b^2}{6}\gamma\frac{\partial \varepsilon_b}{\partial x}\Big|_{x=x_1} + \frac{G}{2t_s}\beta\Big(\int \varepsilon_a\, dx - \beta\int \varepsilon_b\, dx\Big)\Big|_{x=x_1} \\ &\frac{E_b t_b^2}{6}\gamma\frac{\partial \varepsilon_b}{\partial x}\Big|_{x=x_2} + \frac{G}{2t_s}\beta\Big(\int \varepsilon_a\, dx - \beta\int \varepsilon_b\, dx\Big)\Big|_{x=x_2} \frac{E_b t_b^2}{6}\frac{\partial \varepsilon_{b3}}{\partial x}\Big|_{x=x_2} \end{aligned} \tag{2.16}$$

The free stress condition for the ends of actuator, $\sigma_a(x_1,t) = \sigma_a(x_2,t) = 0$, requires that

$$\varepsilon_a(x_1,t) = \lambda \qquad \varepsilon_a(x_2,t) = \lambda \tag{2.17}$$

The dynamic equations (Eqs (2.11) and (2.12)) and boundary conditions (Eqs (2.13) $\div$ (2.17)) formulate a boundary value problem solution which gives the dynamic strain response of the system to the voltage loading of the actuator.

3. Solution to the boundary value problem

The steady-state responses are analysed so the voltage applied to the piezoceramic actuator as well as the strain λ is assumed to be a harmonic single frequency function

$$\lambda = \lambda_0 \exp(\mathrm{i}\omega t) \tag{3.1}$$

On this assumption the solutions of dynamic strain equations are harmonic with the same angular velocity as the excitation

$$\varepsilon_j(x,t) = \varepsilon_j(x)\exp(\mathrm{i}\omega t) \tag{3.2}$$

where the subscript $j = a, b, b_1, b_3$.

Substituting for ε_j into the dynamic equations (Eqs (2.11) $\div$ (2.12)), the system of ordinary differential equations is obtained. The solutions in spatial domain can be expressed in the form (cf Tylikowski (1993))

$$\begin{aligned}
\varepsilon_a(x) &= \sum_{n=1}^{6} C_n \exp(k_n x)\\
\varepsilon_b(x) &= \sum_{n=1}^{6} C_n \alpha(k_n,\omega)\exp(k_n x)\\
\varepsilon_{b1}(x) &= C_7\exp(k_7 x) + C_8\exp(-k_7 x) + C_9\exp(\mathrm{i}k_7 x) + C_{10}\exp(-\mathrm{i}k_7 x)\\
\varepsilon_{b3}(x) &= C_{11}\exp(k_7 x) + C_{12}\exp(-k_7 x) + C_{13}\exp(\mathrm{i}k_7 x) + C_{14}\exp(-\mathrm{i}k_7 x)
\end{aligned} \tag{3.3}$$

where the wavenumbers k_n $(n = 1, 2, ..., 6)$ are calculated from the following algebraic equation

$$\begin{aligned}
&k_n^6 \frac{E_b t_b^2}{12\beta}\gamma E_a t_a - k_n^2\Big[\frac{G t_b}{4 t_s}\Big(E_a t_a \beta + \frac{E_b t_b}{3\beta}\gamma\Big) - \rho_a \frac{E_b t_b^2 t_a}{12\beta}\gamma\omega^2\Big] +\\
&-k_n^2\omega^2\Big(\rho_a \frac{G t_a t_b \beta}{4 t_s} + \rho_c \frac{E_a t_c t_a}{t_b \beta}\Big) - \rho_c \frac{t_c}{t_b\beta}\omega^2\Big(\rho_a t_a \omega^2 - \frac{G}{t_s}\Big) = 0
\end{aligned} \tag{3.4}$$

the amplitude coefficient $\alpha(k_n,\omega)$ is defined as

$$\alpha(k_n,\omega) = \frac{1}{\beta}\Big(1 - \frac{E_a t_a t_s}{G}k_n^2 - \frac{\rho_a t_a t_s}{G}\omega^2\Big) \tag{3.5}$$

and the wavenumber relates to the beam sections 1 and 3 has the form

$$k_7 = \sqrt[4]{\frac{12\rho_b\omega^2}{E_b t_b^2}} \tag{3.6}$$

The fourteen unknown coefficients $C_1, C_2, ..., C_{14}$ are calculated from the system of algebraic equations determined by the boundary, continuity and free stress conditions given by Eqs (2.13) $\div$ (2.17).

After itegrating the formulae for strain $\varepsilon_a(x)$ and $\varepsilon_b(x)$ with respect to x and substituting into Eq (2.10), following distribution of shear stress in the bonding layer is obtained

$$\tau(x) = \frac{G}{t_s} \sum_{n=1}^{6} \frac{C_n}{k_n} [1 - \beta \alpha_n(k_n, \omega)] \exp(k_n x) \tag{3.7}$$

4. The control system transfer functions

The system dynamic response can be expressed in terms of a transfer function. The transfer function relating the beam deflection to the harmonic strain excitation λ is formulated due to the geometric relation given by Eq (2.6) by integrating the strain responses $\varepsilon_b(x)$, $\varepsilon_{b1}(x)$, $\varepsilon_{b3}(x)$ and substituting the strain amplitude $\lambda_0 = 1$

$$G_w(x,\omega) = \begin{cases} -\frac{2}{t_b k_7^2}\left(C_7 e^{k_7 x} + C_8 e^{-k_7 x} - C_9 e^{ik_7 x} - C_{10} e^{-ik_7 x}\right) & x \in (0, x_1) \\ -\frac{2}{t_b} \sum_{n=1}^{6} \frac{C_n}{k_n} \alpha(k_n, \omega) e^{k_n x} & x \in (x_1, x_2) \\ -\frac{2}{t_b k_7^2}\left(C_{11} e^{k_7 x} + C_{12} e^{-k_7 x} - C_{13} e^{ik_7 x} - C_{14} e^{-ik_7 x}\right) & x \in (x_2, l) \end{cases} \tag{4.1}$$

Deflection of the structure develops the strain in the sensor. The thinness of piezofilm and perfect bonding let us assume the uniform distribution of strain, the value of which is the same as that on the surface of the beam. The piezofilm response to the applied strain $\varepsilon_s = \varepsilon_b$ is the charge density (cf Alberts and Colvin (1991))

$$q(x,t) = \frac{k_{31}^2}{g_{31}} \varepsilon_b(x,t) \tag{4.2}$$

where k_{31} and g_{31} is the piezoelectric electromechanical coupling constant and the stress constant, respectively.

Assuming a rectangular shape of the sensing element and its surface electrode identified by the following distribution function

$$\lambda(x) = b[H(x - x_1) - H(x - x_2)]$$

the total charge induced on the surface electrode is represented by the integral on the length of the sensor

$$Q(t) = b \int_{x_1}^{x_2} q(x,t)\, dx \tag{4.3}$$

Substituting Eqs (4.2), (3.2), $(3.3)_2$ into Eq (4.3), using the charge-voltage relation and eliminating time t, the transfer function between the generated voltage and the input actuator strain λ is formulated

$$G_s(\omega) = C_s \sum_{n=1}^{6} \frac{C_n}{k_n} \alpha(k_n, \omega)[\exp(k_n x_2) - \exp(k_n x_1)] \tag{4.4}$$

where C_s is the sensor constant defined as

$$C_s = \frac{k_{31}^2}{g_{31} C_0 (x_2 - x_1)}$$

and C_0 is the capacitance of the unit area.

To obtain active damping of vibrations of the considered system the velocity feedback is applied. The signal of the feedback control loop is proportional to the time derivative of the voltage generated by the sensor. The open-loop transfer function is a product of the transfer function G_s (Eq (4.4)) and the transfer function corresponding to the differentiator

$$G_0(\omega) = \mathrm{i}\kappa\omega G_s(\omega) \tag{4.5}$$

where κ is the gain factor.

The closed-loop transfer function of the active damping system is determined by the well-known formula

$$G_c(x,\omega) = \frac{G(x,\omega)}{1 + G_0(\omega)} \tag{4.6}$$

and relates the beam deflection with feedback loop to the excitation given by actuator strain λ.

5. Results

Calculations have been done for the simply supported steel beam of length $l = 380\,\mathrm{mm}$, width $b = 40\,\mathrm{mm}$ and thickness $t_b = 2\,\mathrm{mm}$. The length of

piezoelectric actuator/sensor pair is $l_p = 38\,\text{mm}$ and its center is located at $x_s = 98\,\text{mm}$. The thickness of piezoceramic actuator and piezofilm sensor is $t_a = 0.2\,\text{mm}$ and $t_f = 0.05\,\text{mm}$, respectively. Material parameters of the system used in calculation are listed in Table 1.

Table 1. Material parameters

Material Parameter	Beam	Actuator PZTG-1195	Sensor PVDF
ρ [kg/m^3]	7800	7280	4500
E [N/m^2]	$2.16 \cdot 10^{11}$	$6.3 \cdot 10^{10}$	$2 \cdot 10^9$
d_{31} [m/V]	-	$1.9 \cdot 10^{-10}$	-
g_{31} [m^2/C]	-	-	0.216
k_{31}	-	-	0.120

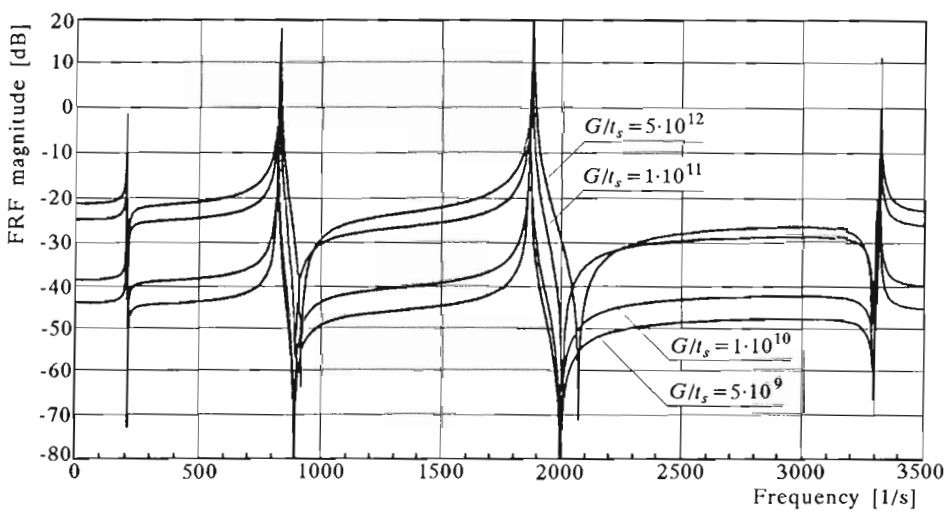

Fig. 3. Beam strain frequency response $\varepsilon_b(\omega)$ for different bonding layer stiffnesses

The dynamic behaviour of the system is represented by means of the frequency response function (FRF). Figure 3 shows the beam strain response ε_b (dB ref.1 strain) to the harmonic input strain λ applied to the actuator the amplitude of which is $\lambda_0 = 1$ (Eqs $(3.3)_2 \div (3.3)_4$). The beam deflection described by magnitude of transfer function G_w, Eq (4.1), is presented in Fig.4. In the both cases the frequency response functions are calculated at $x = 100\,\text{mm}$ which is in the area where the piezoceramic element is located. To predict the influence of the bonding layer properties the shearing stiffness

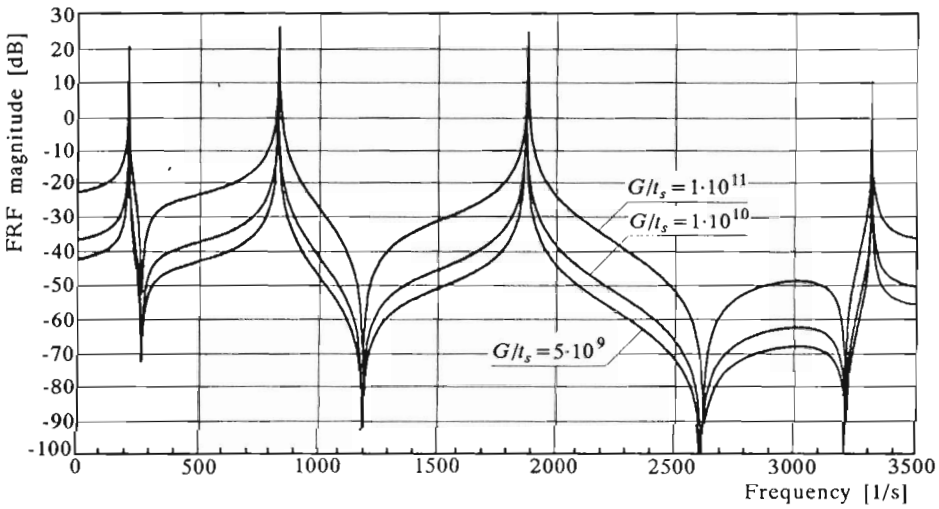

Fig. 4. Magnitude of the transfer function G_w (beam deflection to strain input ratio)

of bonding layer expressed by relation G/t_s is assumed to be of the following values $G/t_s = 5 \cdot 10^9$, 10^{10}, 10^{11}, $10^{12}\,\mathrm{N/m^3}$. It can be seen that both the strain and deflection magnitude plots are characterized by the poles that occur at all resonance frequencies within the observed range. Calculations show that the beam strain as well as the transverse displacement increase when the bonding layer parameter G/t_s becomes greater. Therefore, the actuator works more effectively for a thin and stiff bonding layer.

The above remarks concern also the diagrams of feedback voltage signal (Eq (4.5)) presented in Fig.5.

The feedback control loop parameter defined as the product of sensor and gain constants has the value $C_s\kappa = 0.4\,\mathrm{V/m}$. Relatively small curvature of the beam in the sensing field for the 1st and 4th modes, where an inflaction point is close to the center line of the sensor, reduces the ability of piezofilm to induce a high voltage.

For the closed control loop with the velocity feedback, the frequency function defined as the ratio of beam deflection to input strain (Eq (4.6)) is shown in Fig.6. The transverse displacement response course differs from the plot obtained for the uncontrolled beam (Fig.4).

When the driving frequency lies within the range of resonance, the active damping occurs and peaks are reduced significantly for all modes. The damping is heavier for the frequency corresponding to high efficiency of the sensor.

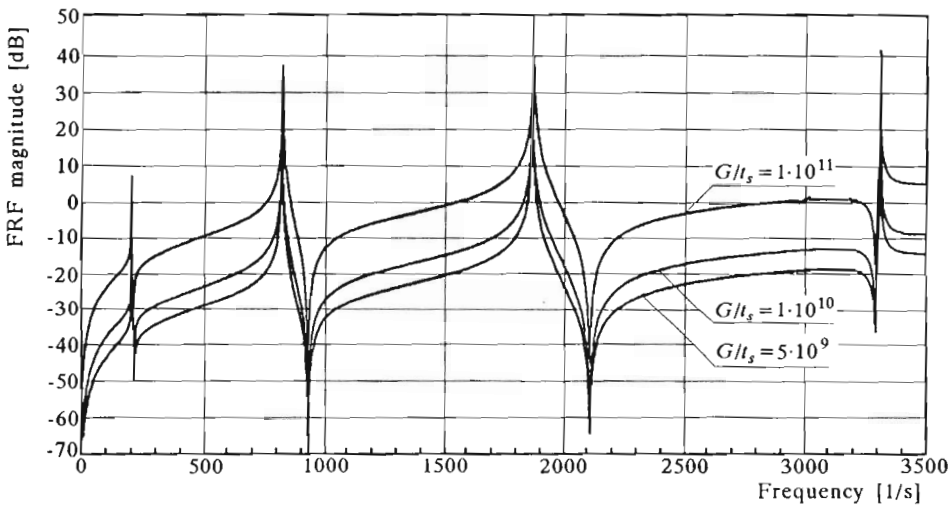

Fig. 5. Magnitude of the open-loop transfer function G_0 (voltage output to strain input ratio)

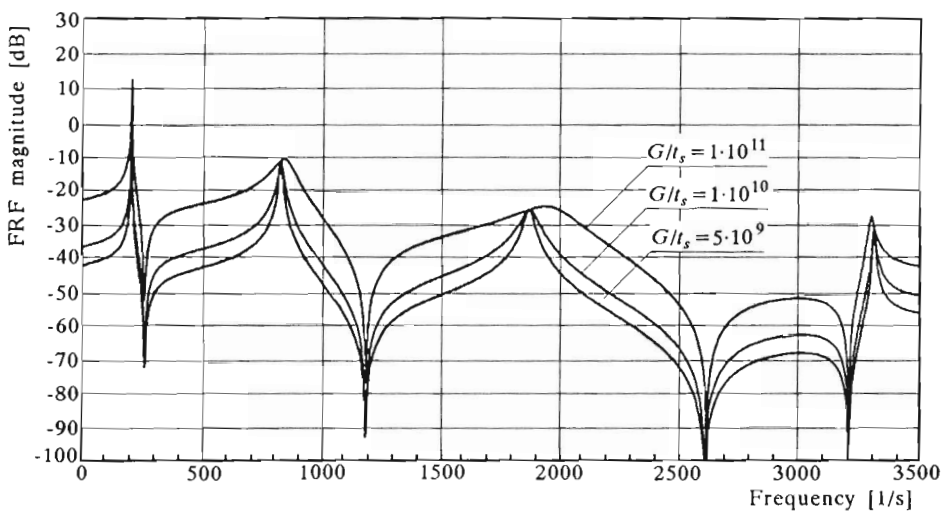

Fig. 6. Magnitude of closed-loop transfer function G_c (ratio of deflection of the controlled system to strain input)

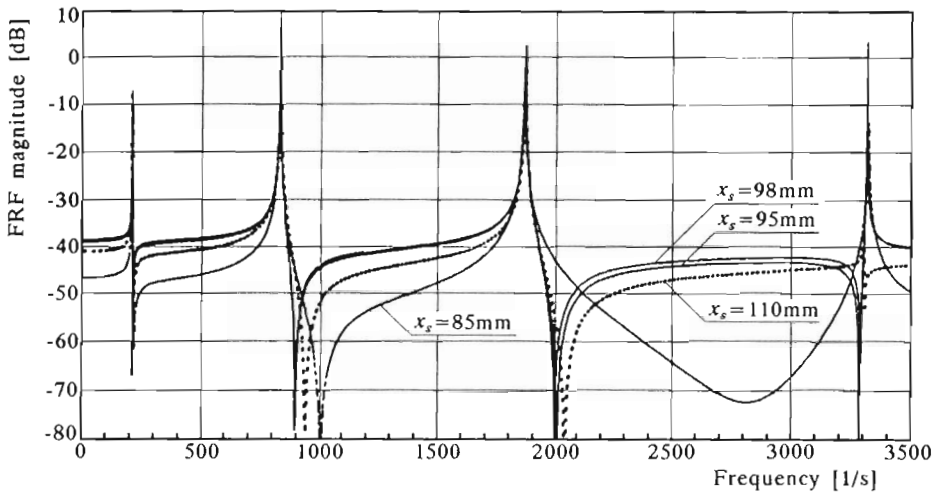

Fig. 7. Influence of the actuator location on the beam strain frequency response $\varepsilon_b(\omega)$ $(G/t_s = 1 \cdot 10^{10}\,\mathrm{N/m^2})$

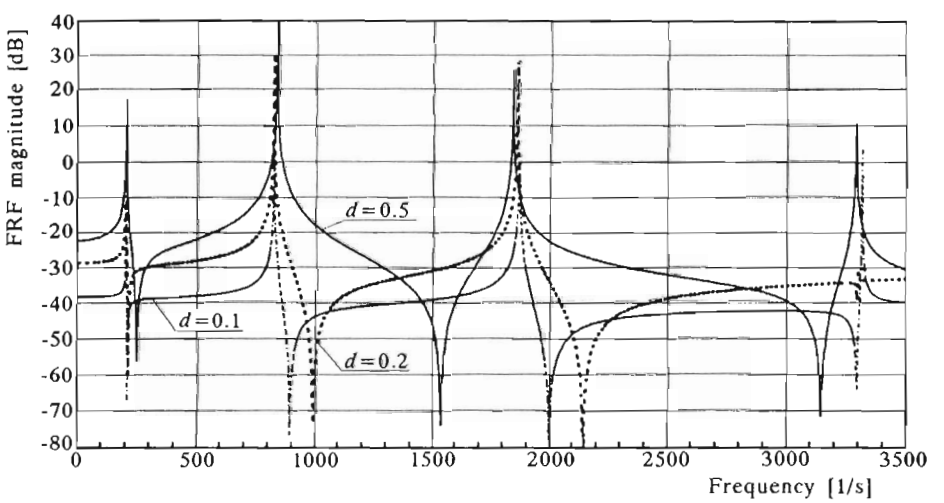

Fig. 8. Influence of the actuator length on the beam strain frequency response $\varepsilon_b(\omega)$ $(G/t_s = 1 \cdot 10^{10}\,\mathrm{N/m2})$

The response of the system depends on the actuator location and its length. In Fig.7 the beam strain frequency functions obtained for several positions of the center line of the actuator, x_s, are shown. The beam strain plots differ significantly for the out of resonance frequencies ($x_s = 85\,\text{mm}$). It can be seen that position of the actuator at $x_s = 110\,\text{mm}$ is not effective to generate the 4th mode of the beam.

The influence of actuator length on the beam strain frequency response is presented in Fig.8. The calculations have been made for the same actuator position given by $x_s = 98\,\text{mm}$. The diagrams show that the increase in the actuator length generally increases the beam strain amplitude, and the change of resonance frequencies can be noticed. Different behaviour of the system is observed for the actuator of length determined by the ratio $d = 0.2$ at the 4th mode when the efficiency of the actuator dramatically diminishes.

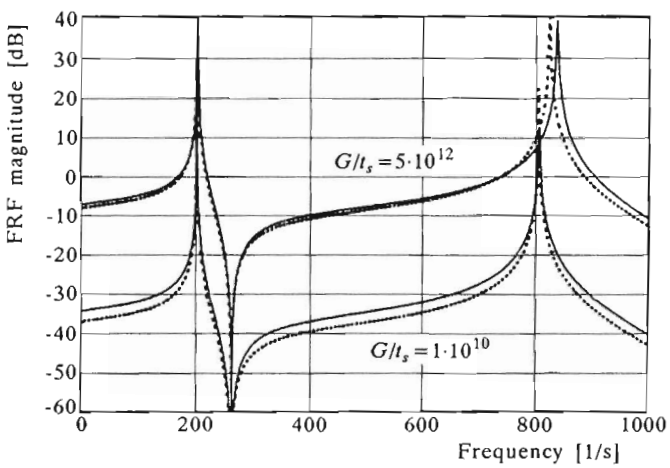

Fig. 9. Influence of bending of the actuator on the uncontrolled beam response

The frequency responses predicted by the present model and by the model where bending of the actuator was neglected, respectively, are compared for the uncontrolled system as well as for the system with the velocity feedback (Fig.9 and Fig.10).

Calculations have been made for two values of the bonding layer parameter $G/t_s = 10^{10}$ and $5 \cdot 10^{12}\,\text{N/m}^3$. In the both figures the solid lines of each pair obtained for the same value of the parameter G/t_s correspond to the present model of the beam-actuator coupling. As it is seen the influence of bending of the actuator is much stronger for smaller values of bonding layer parameter (e.g. for $G/t_s = 10^{10}\,\text{N/m}^3$), especially when the frequency

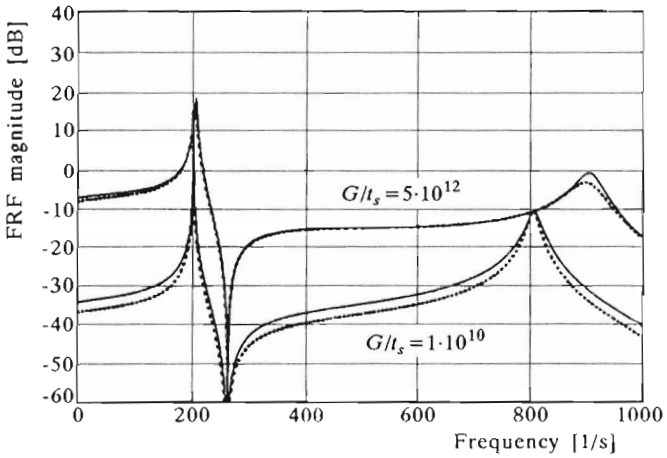

Fig. 10. Influence of bending of the actuator on the controlled beam response

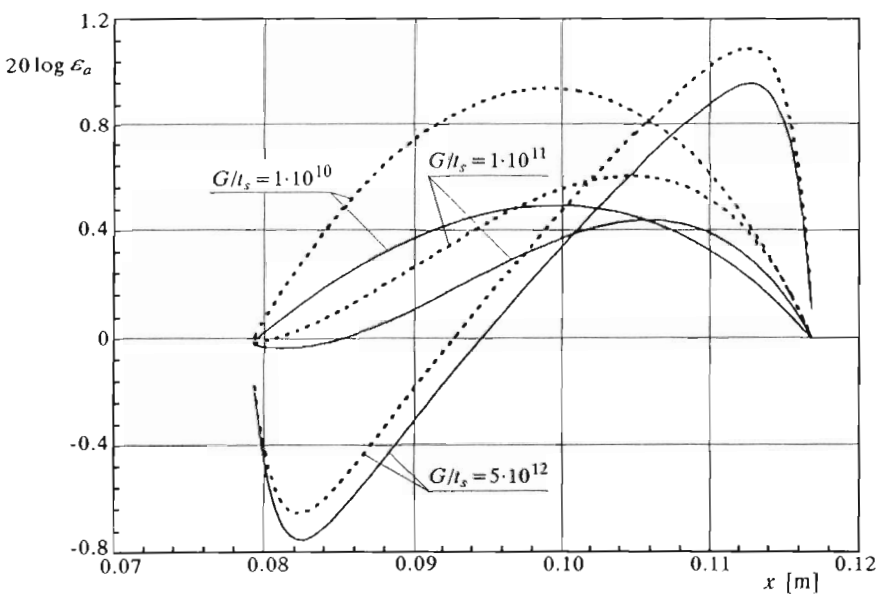

Fig. 11. Comparison of actuator strain distributions at the first resonance frequency

is out of resonance. An another difference causes by involving the bending model of the piezoceramic element is the change of mode frequencies. This effect can be clearly observed for the system with a relatively stiff coupling ($G/t_s = 5 \cdot 10^{12}\,\mathrm{N/m^3}$) within the range of the second resonance frequency.

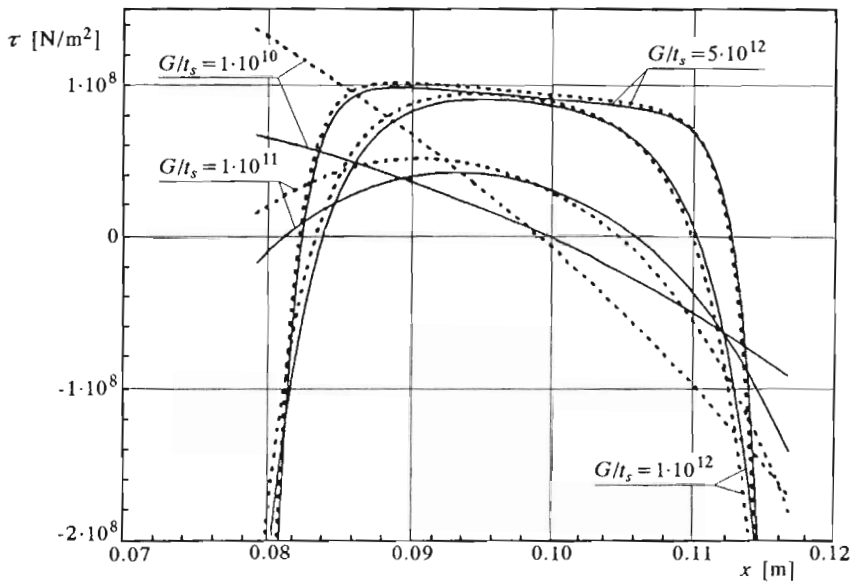

Fig. 12. Comparison of shear stress distributions at the first resonance frequency

Fig.11 and Fig.12 show the actuator strain and shear stress distributions, respectively, which have been obtained for the present (solid lines) and previous (dotted lines) models of the beam-actuator coupling at the first resonance frequency. The model, in which bending of the actuator is introduced gives the actuator strain reduction for all values of the parameter G/t_s used in calculations. Bigger differences between the actuator strain as well as shear stress distributions can be seen for the smaller bonding layer stiffness when the driving frequency is much closer to the modal frequency of the system.

6. Conclusions

The piezoelectric sensor/actuator pair capable of sensing and controlling structural vibrations of a simply supported beam has been theoretically analysed. The dynamic model of the beam-actuator coupling including a bonding

layer has been developed by taking into account the bending effect of the piezoceramic actuator.

The transfer functions for the system with and without velocity feedback control, respectively, have been examined.

Calculations trace the influence of bonding layer properties as well as the actuator location and actuator length on the frequency response. Generally, if an actuator is long and mounted to the substructure by a stiff bonding layer is works more effectively. But the length of the actuator as well as its location can change the actuator ability to generate some modes.

The results based on the proposed model of dynamic coupling are compared with those where the bending of the actuator is neglected. Introduction of the bending causes an increase in the response amplitude as well as a change of mode frequencies which is more significant for more stiff coupling. The influence of actuator bending is proved by the analysis of the actuator strains and shear stresses in the bonding layer.

Acknowledgement

The study was supported by the State Committee for Scientific Research (Grant KBN – No. 3 P404 009 07)

References

1. BAILEY T., HUBBARD J.E., 1985, Distributed Piezoelectric-Polymer. Active Vibration Control of a Cantilever Beam, *Journal of Guidance, Control and Dynamics*, **8**, 605-611

2. CLARC R.L., FULLER CH.R., WICKS A., 1991, Characterization of Multiple Piezoelectric Actuators for Structural Excitation, *J. Acoust. Soc. Am.*, **90**, 346-357

3. CRAWLEY E.F., DE LUIS J., 1987, Use of Piezoelectric Actuators as Elements of Intelligent Structures, *AIAA J.*, **25**, 1373-1385

4. JIE PAN, HANSEN C.H., SNYDER S.D., 1991, A Study of the Response of a Simply Supported Beam to Excitation by a Piezoelectric Actuator, *Proceedings of the Conference on Recent Advances in Active Control of Sound and Vibration*, Virginia, 39-49

5. LEE C.K., CHIANG W.W., O'SULLIVAN T.C., 1991, Piezoelectric Modal Sensor/Actuator Pairs for Critical Active Damping Vibration Control, *J. Acoust. Soc. Am.*, **90**, 374-384

6. NEWMAN M.J., 1991, Distributed Active Vibration Controllers, *Proceedings of the Conference on Recent Advances in Active Control of Sound and Vibration*, Virginia, 579-592

7. PIETRZAKOWSKI M., 1993, Active Vibration Control of One-Dimensional Piezoelectric Laminates, *J. of Theoretical and Applied Mechanics*, **31**, 3, 637-655

8. TYLIKOWSKI A., 1993, Dynamics of Laminated Beams with Active Fibers, *Proceedings of the 3rd Polish-German Workshop on Dynamical Problems in Mechanical Systems*, 67-77

Dynamiczny model połączenia belki i piezoelektrycznego członu wykonawczego w aktywnym sterowaniu drganiami

Streszczenie

Praca dotyczy sterowania drganiami belki swobodnie podpartej przy pomocy elementów piezoelektrycznych tworzących zespół pomiarowo-wykonawczy. W analizie przyjęto dynamiczny model połączenia członu wykonawczego z belką, w którym uwzględniono, oprócz ścinanej warstwy łączącej, także zginanie elementu piezoelektrycznego. Rozwiązując zagadnienie brzegowe oraz zakładając harmonicznie zmienne napięcie zasilające człon wykonawczy, wyznaczono przepustowości widmowe układu głównego bez sprzężenia zwrotnego i układu zamkniętego z prędkościowym sprzężeniem zwrotnym. Na podstawie wyników obliczeń pokazano wpływ właściwości warstwy łączącej na charakterystyki amplitudowo-częstościowe układu. Porównano także reakcję układu w przypadku zastosowania zaproponowanego modelu połączenia z reakcją właściwą modelowi, w którym nie uwzględniono zginania członu wykonawczego.

Manuscript received June 11, 1996; accepted for print September 12, 1996